Bioprinting 25 (2022) e00187

Contents lists available at ScienceDirect

Bioprinting

journal homepage: www.sciencedirect.com/journal/bioprinting

2D Nanosilicate for additive manufacturing: Rheological modifier, sacrificial ink and support bath

Satyam Rajput [a], Kaivalya A. Deo [a], Tanmay Mathur [a], Giriraj Lokhande [a], Kanwar Abhay Singh [a], Yuxiang Sun [b], Daniel L. Alge [a,c], Abhishek Jain [a,g,h], Tapasree Roy Sarkar [d], Akhilesh K. Gaharwar [a,e,f,*]

[a] Department of Biomedical Engineering, College of Engineering, Texas A&M University, College Station, TX, 77843, USA
[b] Nutrition, College of Agriculture and Life Sciences, Texas A&M University, College Station, TX, 77843, USA
[c] Department of Material Science and Engineering, College of Engineering, Texas A&M University, College Station, TX, 77843, USA
[d] Department of Biology, Texas A&M University, College Station, TX, 77843, USA
[e] Interdisiplinary Program in Genetics, Texas A&M University, College Station, TX, 77843, USA
[f] Center for Remote Health Technologies and Systems, Texas A&M University, College Station, TX, 77843, USA
[g] Department of Medical Physiology, College of Medicine, Texas A&M Health Science Center, Bryan, TX, 77807, USA
[h] Department of Cardiovascular Sciences, Houston Methodist Institute for Academic Medicine, Houston Methodist Research Institute, Houston, TX, 77030, USA

ARTICLE INFO

Keywords:
3D printing / bioprinting
Additive manufacturing
Biomaterials ink
Nanoparticles
Regenerative medicine

ABSTRACT

Extrusion-based 3D printing/bioprinting is a promising approach to generate patient-specific tissue engineered grafts. However, a major challenge in extrusion-based 3D printing/bioprinting is that most currently used materials lack the versatility to be used in a wide range of applications. In this study, we introduce colloidal solutions of two-dimensional (2D) nanosilicates as a platform technology to print complex structures *via* three different approaches. In the first approach, we designed a shear-thinning ink composed of nanosilicates, which can be further reinforced by adding different types of water-soluble polymers. In the second approach, we demonstrated the use of nanosilicates as a sacrificial ink to design microfluidic devices for *in vitro* disease modelling. In the third approach, we utilized a colloidal nanosilicate gel as a support bath for 3D printing by nullifying the surface tension and gravitational forces. Due to their exceptional versatility, nanosilicate-based biomaterials could be widely adopted in the fields of additive manufacturing, tissue engineering, drug delivery, and medical devices.

1. Introduction

Additive manufacturing has emerged as a powerful tool in the field of tissue and organ engineering in the past decade. The ability to construct structures with a bottom-up approach gives additive manufacturing a distinct advantage compared to traditional methods [1]. While a variety of approaches have been developed, extrusion-based 3D printing has been widely adopted by biomedical researchers worldwide due to its simplicity of use, low cost, open source nature, high precision in depositing materials, and compatibility with a wide variety of soft materials/hydrogels [2]. Extrusion-based 3D printing concurrently demands several properties from hydrogels to be useful for ink or bioink (cell-laden ink). To qualify as an ideal ink (or bioink), the following properties of a hydrogel should be optimized: (a) shear-thinning and self-recovery characteristics to facilitate extrusion and printing of ink formulation; (b) high mechanical strength to sustain printing of multiple layers; and (c) appropriate biological properties to support cell adhesion proliferation and remodeling [3,4]. It is difficult to achieve all these characteristics using conventional single-component hydrogels. Hence, the last decade has seen an exponential growth in the number of studies focused on development of biomaterials-based ink or bioink for extrusion-based 3D printing [5]. In pursuit of ideal inks, researchers have employed various techniques such as the use of polymer functionalization/dual crosslinking hydrogel mechanisms [6], supramolecular hydrogels [7], interpenetrating network hydrogels [8], nanocomposite hydrogels [9], click chemistry [10], and co-printing or thermoplastic

* Corresponding author. Department of Biomedical Engineering, College of Engineering, Texas A&M University. 3120 TAMU, 5024 754 Emerging Technology Building, College Station, TX, 77843- 755 3120, USA.
E-mail address: gaharwar@tamu.edu (A.K. Gaharwar).

https://doi.org/10.1016/j.bprint.2021.e00187
Received 23 August 2021; Received in revised form 2 December 2021; Accepted 20 December 2021
Available online 8 January 2022

reinforcement [4,11]. Despite the advances in various techniques, it is very difficult for a single technique to be used for a variety of applications [12].

To overcome these drawbacks, one of the major strategies is to use a rheological additive/modifier to improve the rheological properties of polymers for 3D bioprinting. Two dimensional (2D) nanoclays such as nanosilicates (also known as Laponite®, BKY additives) have been used as a rheological modifier for designing bioinks [13]. These nanosilicates have been investigated for a variety of biomedical applications such as tissue engineering, drug delivery, wound healing [14]. Nanosilicates are disc-shaped inorganic nanoparticles that are 20–50 nm in diameter and 1–2 nm in thickness. The empirical formula for nanosilicates is $Na^{+0.7}[(Si_8Mg_{5.5}Li_{0.3})O_{20}(OH)_4]^{-0.7}$ and they are characterized by their unique charge distribution. When exfoliated in deionized (DI) water, nanosilicates develop partial negative charges on the faces and partial positive charges on the edges, which enables the nanosized particles to form a colorless, clear colloidal viscoelastic gel [15]. Nanosilicates form a "*house-of-cards*" structure above a certain concentration in DI water [16]. This structure imparts appealing rheological properties such as increased viscosity and yield stress, as well as shear thinning and thixotropic behavior [17]. The rheological properties can be easily tuned by varying the concentration of nanosilicate, which makes it very useful for extrusion-based 3D printing [18]. Moreover, the benign nature of nanosilicates towards biological entities makes them a suitable candidate for tissue engineering [19–22].

Another challenge with soft material 3D printing is the printing of vessels or vasculature inside 3D printed construct. The last decade has seen great growth in organ-on-a-chip based microfluidics to mimic the physiology of various organs, especially the vasculature [23]. However, the studies usually use polydimethylsiloxane (PDMS) or polycarbonate to fabricate the organ-on-a-chip devices. These materials are inherently bioinert and inhibit diffusion of nutrients and biomolecules though them due to the high material density [24]. An adequate nutrient supply and the diffusion of gases (oxygen and carbon dioxide) are important for maintaining cell viability and the proper function of tissues and organs [25, 26]. As a result, hydrogel-based microfluidic devices have been studied to provide 3D cell culture environments incorporating the use of sacrificial inks. Alginate, agarose, wax, carbohydrate glass, pluronic F127, petroleum jelly-liquid paraffin [27] and gelatin have been used as sacrificial inks [28]. Unfortunately, most of these techniques require complex pre-processing and post-processing and forming complex microchannels is difficult. Hence, we have investigated the use of nanosilicates as a sacrificial ink to fabricate hydrogel-based microfluidics.

Another major challenge in extrusion-based 3D printing is the ability to print tall and complex structures with overhangs because soft materials flow under gravity and cannot form self-supporting structures. Recently, an advancement in 3D printing called sacrificial support bath printing has been developed to circumvent this challenge [29]. The sacrificial support bath method uses a responsive rheological support bath to deposit soft material inside the gel like medium, which is removed (sacrificed) after the printed soft material is crosslinked. The support bath helps in printing tall and complex structures as it reduces or nullifies the external forces of surface tension, gravity and inertia [30]. These forces lead to unsuccessful printing of tall and complex structures of soft materials for extrusion-based printing with air as medium. This technique has even been used for multimaterial extrusion printing [31]. Different materials such as gelatin microparticles [32], jammed hydrogels [33], and polysaccharides [34] have been used as support bath materials, but each suffers from some type of limitation. Gelatin microparticles are sensitive to temperature, and cells may undergo a thermal shock when they are liquified >37 °C. Jammed microgels or Carbopol (acrylic polymers) are sensitive to ionic solutions. Polysaccharides might interact with printed structures and make it difficult to print precise structures. In general, support bath materials are shear thinning and show yield strength and thixotropic behavior. Thus, due to their tunable rheological properties, we investigated the use of nanosilicates as a support bath in this study.

In this study, we demonstrate the versatility of two-dimensional (2D) nanosilicates/nanoclay as a platform technology for additive manufacturing *via* three different approaches. In the first approach, we will design a shear-thinning ink composed of nanosilicates, which can be reinforced by adding different types of water-soluble polymers to nanosilicate solution. In the second approach, we will demonstrate the use of nanosilicates as a sacrificial ink to design hydrogel based microfluidic devices for *in vitro* disease modelling. In the third approach, we will utilize a colloidal nanosilicate gel as a support bath for 3D printing by nullifying the surface tension and gravitational forces.

2. Experimental section

2.1. Materials and methods

Nanosilicates (Laponite XLG) were sourced from BYK Additives Inc, USA. Porcine based gelatin (Type A, Bloom No. 300), Irgacure 2959 (2-Hydroxy-4′-(2-hydroxyethoxy)-2-methylpropiophenone), and methacrylic anhydride were purchased from Sigma-Aldrich (USA). Kappa Carrageenan (κCa) was purchased from TCI Chemicals. Gelatin methacryloyl (GelMA) was synthesized by a previously described method [35]. In short, GelMA (75–80% methacrylolated) was prepared by dissolving 10 g of gelatin in 100 mL of heated (60 °C) phosphate buffered saline (PBS) solution for an hour. Once gelatin was dissolved, 8 mL methacrylic anhydride was added to the mixture at a rate of 1 ml/min. After stirring the solution at for 3 h at 60 °C, 400 mL of 1X PBS was added. This prepared solution mixture was dialyzed at 50 °C for 7 days, frozen at −80 °C and lyophilized. The degree of methacryloylation (Fig. S1) was calculated using a previously described method [36]. Nanosilicate ink solutions were prepared by adding Nanosilicates in deionized (DI) water (18.2 MΩ) and vortexing vigorously for 2 min. They were exfoliated for 24 h and used for further experiments.

2.2. Rheological characterization

The rheological tests were performed on a TA Instruments Discovery Hybrid Rheometer (DHR-2) equipped with a 20 mm parallel plate geometry. The geometry gap was kept as 400 μm and the experiments were performed at 25 °C. Precursor solutions of exfoliated Nanosilicates at different concentrations were used. Rotational sweep tests were performed between 10^{-1} s^{-1} and 10^{2} s^{-1} to determine the yield stress and power law index constants, n and K *via* the use of TRIOS software from TA Instruments. Peak hold tests were performed by keeping the shear rate at 10^{-2} s^{-1} for 60 s, 3000 s^{-1} for 5 s and 10^{-2} s^{-1} for 180 s to mimic the behavior of the ink inside a nozzle. The time for 80% viscosity recovery was calculated manually. Peak hold tests for 4 cycles were performed to evaluate viscosity recovery after multiple cycles. Frequency sweeps were performed between 10^{-2} to 10^{2} Hz and stress sweeps were performed. Also, amplitude sweeps were performed with oscillatory amplitude varying from 0.1 to 2000 Pa. The frequency was varied between 0.1 Hz and 100 Hz. G' values at 1 Hz, 1 Pa from stress sweep and at 1 Pa, 1 Hz were plotted to see the trend in storage modulus. Moreover, temperature sweeps were performed to quantify the dependence of different concentrations on temperature. The temperature was varied from 25°C to 85 °C.

2.3. Imaging

Imaging was done using a Zeiss Stereomicroscope and DSLR camera Nikon D3500. The morphological characterization of the hydrogel samples was performed by scanning electron microscopy (SEM) using a NeoScope JCM-5000 SEM equipment. To prepare the hydrogel samples, liquid nitrogen was used to flash freeze them. They were cut using a razor blade, and then lyophilized. The cut samples were sputter-coated

with gold to a thickness of 20 nm and imaged using SEM.

2.4. 3D printing

A custom modified Anet A8 printer was used to extrude viscoelastic ink formulations. Commercially available thermoplastic 3D printer Anet A8 was modified to print hydrogels and soft materials. For this, the thermoplastic head was removed and a custom extruder head for printing soft materials or hydrogels was 3D printed and attached to a screw-based piston extruder. The control system was also replaced by changing the microcontroller and using the open-source Arduino Uno microcontroller. All 3D designs were made in Solidworks and saved as. stl files. These files were exported to 3DSlicer, which is an open-source program. The 3DSlicer program cuts the design in layers and generates G-code, which is read by the 3D printer and dictates the movement of different motors. Another open-source software called Repetier host was used as the interface for 3DSlicer. When printing on a hard surface in air, a 22-gauge plastic tapered nozzle was used. The printing speed was kept at 10 mm/s unless specified otherwise. The flow rate was 0.1 mL/min.

The structures were designed in Solidworks software (Dassault Systèmes) and converted to an stl file. The stl file was then imported to Repertier Host software. The structures were modified and sliced using Slicer software to generate G-code for printing path of the printer head. A 22 gauge nozzle was used for all the prints. The layer thickness was 200 μm. All prints were carried out at room temperature. Some of the stl files were downloaded from different sources and modified to be printed: human femur (https://3dprint.nih.gov/discover/3dpx-000168), human anatomical heart (https://www.thingiverse.com/thing:932606), DNA structure (https://www.thingiverse.com/thing:1810631), and trileaflet heart valve (https://3dprint.nih.gov/discover/3dpx-000452).

2.5. Drug release studies

Drug release from nanosilicate was demonstrated for 3D printed grid structures of 6% nanosilicate loaded with different doxorubicin (Dox.) concentrations ranging from 100 to 800 μm/ml. These grid structures were then exposed to MDA-MB-231 cells for 24 h to observe the effect of doxorubicin on cell growth. In order to demonstrate the synergistic effect of two drugs [BMS-777607 (tyrosine kinase inhibitor; Cayman Chemicals, #18517) [37] and LGK794 (Wnt inhibitor; Cayman Chemicals, #14072)] [38], MDA-MB231 cells were chosen, as these cells are characterized by overexpression of the receptor tyrisone kinase (RTK) [39] and Wnt [40]. Due to the existence of cancer stem cells, triple negative breast cancer (TNBC) cells develop chemo resistance and relapse after treatment. Therefore, targeting abnormal signal pathways to eliminate cancer stem cells (CSCs) might be a promising strategy to manage TNBC. As the TGF-β, Notch, Wnt/β-catenin signaling pathways and tyrosine-kinase receptors are deregulated in TNBC cells (such as MDA-MB-231), targeting one or more signaling pathway can have synergistic inhibitory effects [41]. The above-mentioned drugs were loaded in nanosilicate to inhibit TNBC cell growth. Twenty-four hours after the treatment, the 3D printed structure was washed with PBS and the cells were fixed with 4% paraformaldehyde. The cells were treated with 0.5% Triton X-100 for permeabilization and mounted with ProlongTM Diamond Antifade Mountant with DAPI (ThermoFisher, #P36966). The synergistic inhibitory effect of BMS-777607 (2.5 μM alone or 1.25 μM combined) and LGK794 (2 nM alone or 1 nM combined) was further validated using Western blots using P21 (Santa Cruz, #sc6246) and cyclin D1(Santa Cruz Biotech, #sc8396) protein level, the inhibition of which is correlated cell cycle arrest [42].

2.6. Fabrication of microfluidic devices

A formulation of 5% GelMA, 5% Gelatin and 0.25% Irgacure 2959 were added to DI water at 50 °C. This formulation was then poured into an acrylic mold and cooled at 4 °C. 6% Laponite XLG was used to print a channel on the cast layer of hydrogel. A layer of heated 5% GelMA +5% Gelatin + Irgacure 2959 formulation was poured on top of the printed channel kept at 4 °C. The whole cast device was then UV crosslinked by a UV lamp. The crosslinked hydrogel device was removed from the mold and Laponite XLG was extracted by flushing PBS through the channel. Laponite XLG was removed by flowing PBS through the channel that disrupts the electrostatic interaction among nanosilicates. Gentle push on the channel of the hydrogel microfluidic device might be required to move the sacrificial ink. Then, fresh PBS formulation is perfused in the channel to continue removing the nanosilicates. We repeated this process multiple times to remove the sacrificial ink.

2.7. Support bath 3D printing

Support bath printing was done in a bath made of 4% Laponite XLG formulation. Laponite XLG was exfoliated in DI water for 24 h and used as a support bath. GelMA and κCa inks were prepared by adding 10% w/v GelMA and 0.8% w/v κCa in DI water at 40 °C. The printing was performed at room temperature using the printer discussed above. 22-gauge blunt metal nozzles purchased from McMaster Carr were used for printing inside the support bath. The printed structures were covalently crosslinked by shining UV light on them. After crosslinking, PBS was used to dilute the support bath and extract the printed structures. They were ionically crosslinked by keeping them inside 5% w/v Potassium Chloride (KCl) solution. The resolution for the 3D printing process was about 400 μm, ie the diameter of the extruded strand. The resolution can be changed by varying the needle size or by changing the extrusion pressure for under-extrusion or over-extrusion.

2.8. Mechanical testing

Uniaxial unconfined compression testing was done on a ADMET MTEST Quattro eXpert 7600 mechanical testing machine. Hydrogel samples were crosslinked and compressed to 50% or 30% their initial height. Stress versus strain curves were plotted in Graphpad prism 8.0 and compressive modulus was calculated. Cylindrical samples of diameter 6 mm and height 3 mm were used. The unconstrained samples were compressed and were allowed to return to their starting position at a rate of 1 mm/min. Raw data generated from the default software was fed into an Excel macro to find the compressive modulus, maximum stress at maximum strain and toughness values. The data was then plotted in Graphpad Prism.

2.9. Computational fluid dynamics (CFD) simulation

Computational Fluid Dynamics (CFD) simulations were performed using ANSYS 19 software. The n and k values from fitting the power law model to the shear rate sweeps were used as input variables in the software. Initial velocity and maximum and minimum viscosity were also used as input variables, and simulations were performed on a Solidworks model of the nozzle.

2.10. In vitro studies

Printed and crosslinked gel discs of 6 mm in diameter and 2 mm in height were placed in a 96-well plate and sterilized using 70% ethanol washes and UV light exposure. Gels were then washed with 1X PBS to remove ethanol. Human umbilical vein endothelial cells (HUVECs) were cultured in tissue culture-treated T-75 flasks supplemented with EGM-2 media with 1% Penstrep until reaching 75% confluency. Once confluent, the cells were detached from the surface using Accutase and seeded on gel discs at a cell density of 20,000 per disc in replicates of 3. EGM-2 media was added to the wells. Cells seeded on TCPS were used as positive controls. Discs were incubated at 37 °C under 5% CO_2 for 24 h. After 24 h, media was removed and discs were washed with 1X PBS. A

10% Alamar blue solution was prepared in EGM-2 media and added to each well containing the gel discs. Solution added to an empty well was used a negative control (blank). The gels were incubated for 2 h at 37 °C under 5% CO_2. After 2 h, the Alamar blue solution was transferred to a fresh well plate and the absorbance at 570 nm was measured. Using the following formula, the viability of cells cultured on gel discs was measured. All values were normalized to the TCPS control.

$$\frac{Absorbance\ of\ sample - Absorbance\ of\ blank}{Absorbance\ of\ TCPS\ control - Absorbance\ of\ blank} \times 100$$

2.11. Statistical analysis

Data are presented as the means ± standard deviations of the experiments (n = 3–5). Statistical analysis was performed using ANOVA with a post-hoc Tukey tests for multiple comparisons. Statistical significance was defined as *$p < 0.05$, **$p < 0.01$ and ***$p < 0.001$.

3. Results and discussion

3.1. Viscosity and rheological characterization of nanosilicate

Nanosilicate has been investigated for biomedical applications as a synthetic biomaterial due to its consistency in shape, size, charge, chemical composition [14]. This consistency is due to the use of synthetic manufacturing processes. We chose to use nanosilicates for this study due to their high biocompatibility. Nanosilicate has a complicated phase diagram as a viscoelastic fluid due to the electrostatic interactions between each phyllosilicate disc [16,43,44]. The first experiment was done to qualitatively characterize the viscous properties of different concentrations of nanodiscs. We used different nanosilicate concentrations from 1-10% w/v in DI water. Nanosilicate gel formulations were made by adding the desired amount of nanosilicate powder to DI water, vortexing for 2–5 min, and letting the nanosilicates exfoliate for 24 h. Exfoliation is the dispersion of nanosilicates from the tactoid stacked geometry to individual particles in water. This happens through the release of Sodium (Na+) ions that are present between the nanosilicates disks from the manufacturing process. The initial experiment was done to assess the self-assembly or self-gelation characteristics of nanosilicate. Different concentrations of nanodisc gels were made in small glass vials and turned upside down after 24 h. Blue food coloring was used to aid visualization. The viscosity of nanosilicate solutions of 3% w/v and above formed a self-supporting gel and did not flow even after gentle tapping of the vial (Fig. 1A). The 1% nanosilicate solution flowed easily on flipping the vial, while the 2% nanosilicate solution flowed only after gently tapping the vial. The concentrations of 3% and above show solid-like viscoelastic behavior due to the formation of a "house--of-cards" structure. This happens by the equilibrium of electrostatic repulsions and van der Waals attractive forces [45]. In terms of energy, this has been attributed to a jammed state, wherein the energy to remain in suspension is reduced by restricting the movement of nanodiscs [15, 46].

Our next goal was to perform rheological characterization of different concentrations of nanodiscs to obtain quantitative data. Rotational shear rate sweeps were performed on various concentrations to assess the behavior with increasing shear rate. This was done to simulate the flow behavior of different nanosilicate concentrations at different shear rates at room temperature (24 °C). The results indicated that all formulations starting from 3% w/v nanosilicates showed shear thinning behavior (decrease in viscosity with increase in shear rate), while 1% and 2% nanosilicates did not show shear thinning behavior (Fig. 1B). These concentrations (1% and 2%) exhibited a Newtonian like behavior, which can be attributed to the lack of interactions between nanodiscs. Formulations of 3% and above behaved as a solid before reaching a yield stress and started flowing after the yield stress, showing a non-Newtonian shear thinning behavior. This shear thinning behavior was modelled by applying a power law on the stress strain curves obtained from shear rate sweeps. The power law model is given by the equation:

$$\eta = K\dot{\gamma}^{n-1}$$

In this equation, η refers to viscosity, K refers to flow consistency index, γ refers to shear rate and n refers to the flow behavior index. On applying this model, values for K and n were obtained and are summarized (Fig. 1B, table).

A value of n less than 1 indicates shear thinning behavior, whereas n greater than 1 indicates dilatant behavior. The addition of nanodiscs caused the value of n to rapidly decrease from 1% concentration to 10% concentration. This was due to the unsettling of the "house-of-cards" structures at higher concentrations and nanodiscs undergoing flow under the applied shear stress. Under shear, the nanodiscs orient themselves parallel to the direction of flow at the micro level, helping to make the colloidal formulation flow easily at the macro level. It has been hypothesized that there is electrostatic repulsion among the nanosilicate particles that makes them easily slide over each other under shear, thereby exhibiting shear thinning behavior [47]. The value of K increased due to increase in nanosilicate concentration as more nanodiscs were packed per unit volume. This resulted in a higher volume of nanodics, leading to higher packing density. Similarly, yield stress values increased with increasing nanosilicate concentration due to increased interparticle interactions resulting in higher packing density of internal house-of-cards structures. Higher yield stress helps the extrudate flow as a viscoelastic solid, which is desirable for extrusion-based 3d printing of soft materials.

Oscillatory rheological measurements were done on different nanosilicates concentrations to simulate the flow of ink and validate the results from rotational sweeps (Fig. 1C–D). The aim of these experiments was to determine the storage modulus (G′) and loss modulus (G″) over different frequencies, amplitudes and, temperatures, and to verify the trends of rotational sweeps. We performed these tests on nanosilicate concentrations from 3% to 10% since it was clear that 1% and 2% were not suitable for 3D printing. Only 4%, 6% and 8% were plotted for better visibility and clarity. First, the amplitude sweeps were performed to verify the trends in yield stress obtained from rotational measurements. The linear viscoelastic region was determined by performing stress sweeps at 1 Hz, 1 Pa (Fig. 1C). It was found that the crossover points (G'<G″) occurred at about 113 Pa, 341 Pa and 850 Pa for 4%, 6% and 8% nanosilicate concentrations. The yield stress trends were similar to that found with rotational tests. Next, the frequency sweep was performed on the various concentrations at 1 Pa, 1 Hz (Fig. 1D). For all nanosilicate formulations, the behavior of G′ and G″ was independent of frequency, which indicated non-Newtonian behavior. Internal structure formation with nanosilicates addition seems to have quashed any dependence of behavior on frequency. Moreover, temperature sweeps were performed to quantify the dependence of different concentrations on temperature. The modulus values, G′ and G″ remained constant over the temperature range of 25°C–85 °C (Fig. 1E). This means that other polymers can be mixed with nanosilicates and can be used at higher temperatures without compromising the properties of the formulation.

3.2. Simulating the printability of nanosilicate

To simulate the behavior of ink during extrusion-based 3D printing, we performed peak hold tests on different concentrations of nanosilicates using a rheometer. Peak hold tests were designed to simulate the three stages of 3D printing - ink flow: (1) inside the barrel, (2) inside the nozzle and, (3) post extrusion. A schematic of the ink behavior during the extrusion process is shown in Fig. 2A. A multiple cycle (4 cycle) peak hold test was performed to see if this behavior was recurrent with each cycle and we found that the viscosity recovery took place after each cycle (Fig. S2). Hence, the formation of internal "house of cards" structure takes place after even being sheared at high shear rates

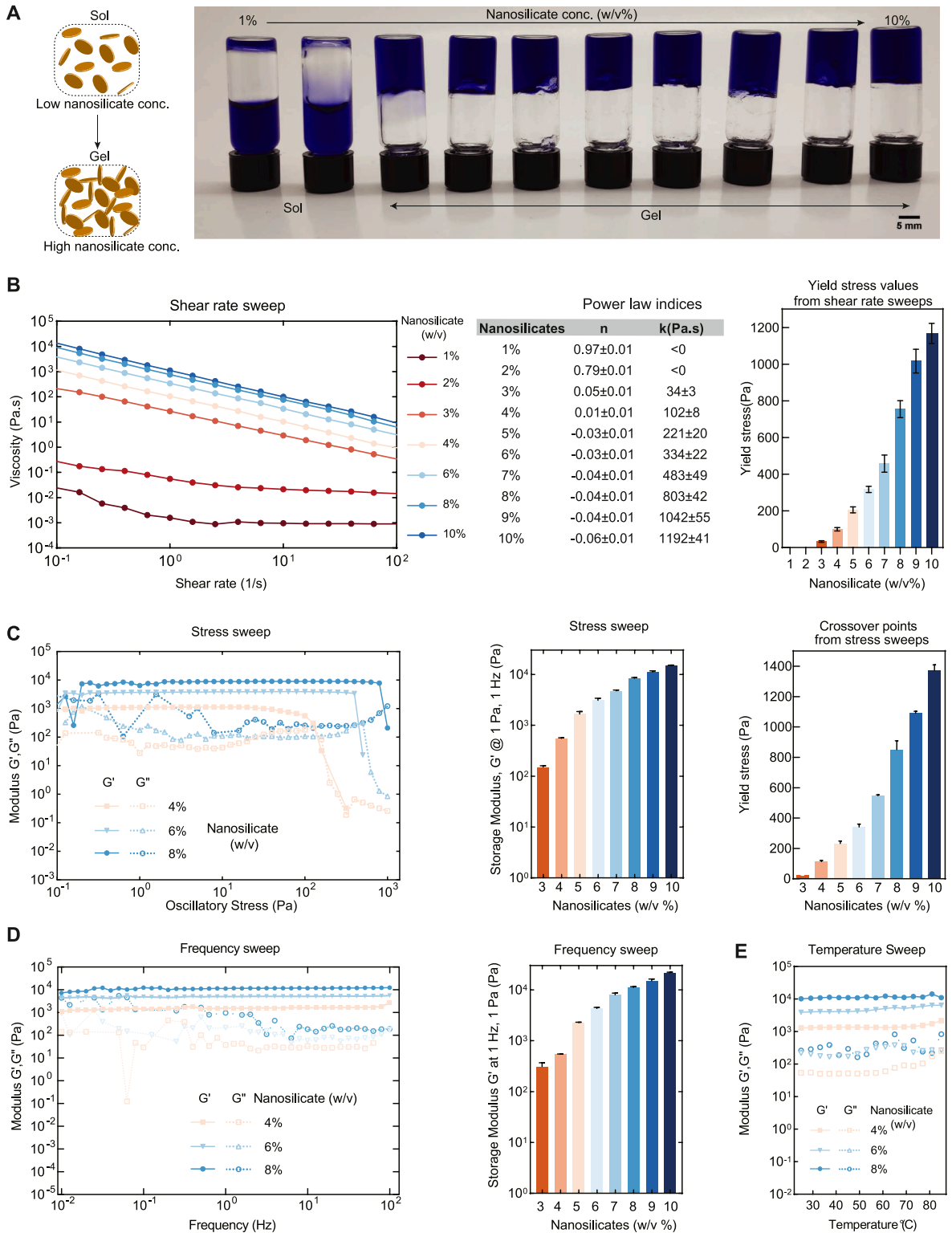

Fig. 1. Effect of nanosilicate concentration on rheological characterization. (A) An increase in nanosilicate concentration results in transformation of colloidal solution from sol to gel state. Qualitative viscosity of different nanosilicate concentrations from 1 to 10% w/v is shown by vial inversion test (scale bar = 5 mm). (B) Rotatory shear sweep of different nanosilicate concentrations from 1 to 10% w/v (some curves are not shown for graph clarity) is shown. The table shows the power law indices that were obtained from the shear rate sweeps data. Yield stress value obtained from shear rate sweep for different nanosilicate concentrations are shown (n = 3–5). (C) Oscillatory stress sweeps from 10^{-1} to 10^{3} Pa obtained for various concentrations of nanosilicate to validate yield trends from shear rate sweeps (only 4%,6% and 8% are shown for graph clarity). The bar graph show storage modulus at 1 Pa and crossover points for yield stress were obtained from stress sweeps data. (D) Frequency sweeps from 10^{-2} Hz–10^{2} Hz (only 4%,6% and 8% are shown for graph clarity) shows non-Newtonian fluid behavior. Storage modulus at 1 Pa from frequency sweeps. (E) Temperature sweeps from 25 °C to 85 °C (only 4%,6% and 8% are shown for graph clarity) demonstrates the temperature independence of different nanosilicate concentrations.

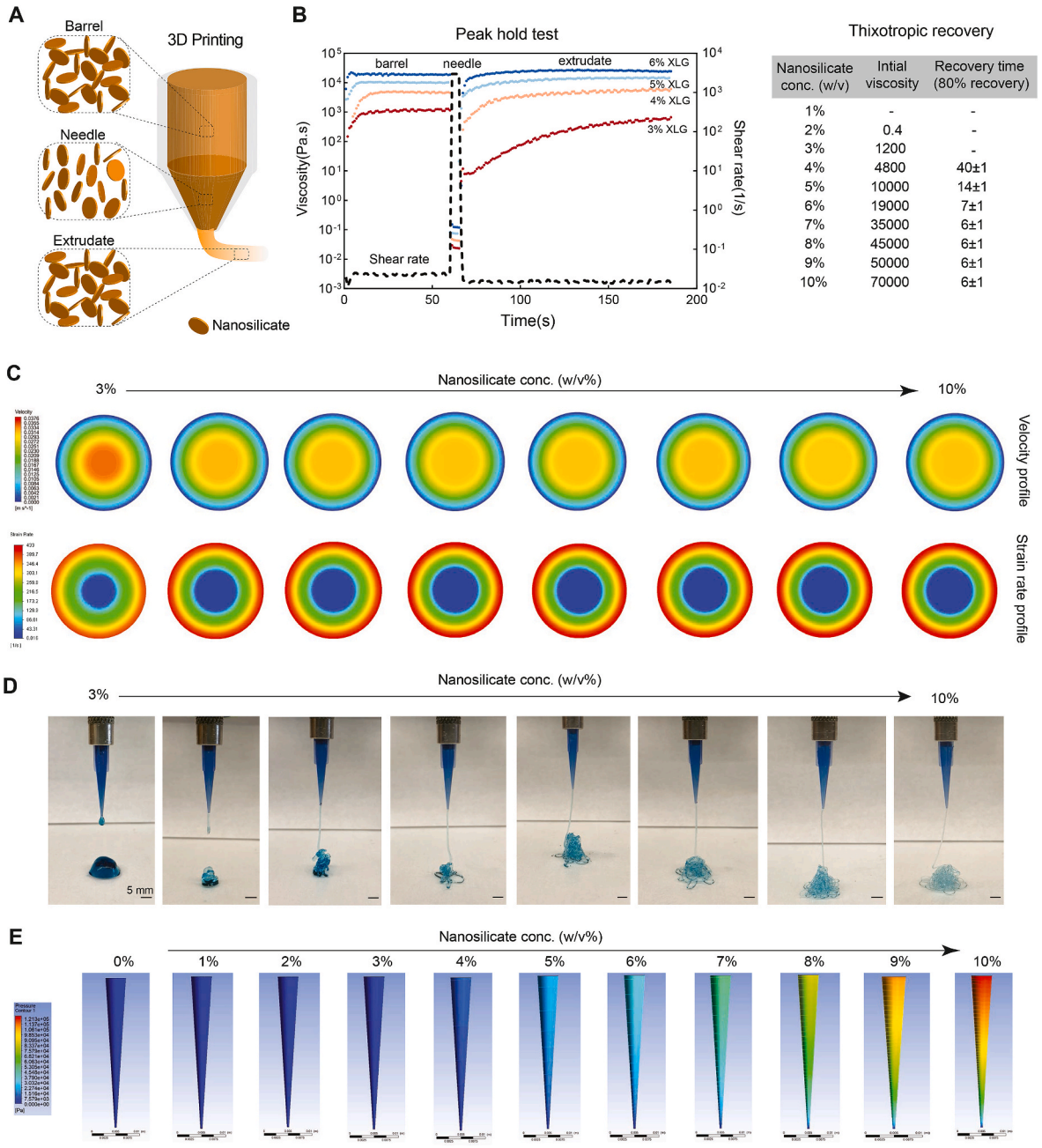

Fig. 2. Simulation of nanosilicate flow through the nozzle using rheometer and computational fluid dynamics (CFD) modelling. (A) Schematic showing the orientation of nanosilicate discs at different locations inside the nozzle during the extrusion process. (B) Peak hold test for different nanosilicate concentrations (not all concentrations are shown for clarity) and corresponding table showing the recovery time for different nanosilicate concentrations for determining the thixotropic behavior (C) CFD profiles of velocity and strain rate at the end of the nozzle for nanosilicate concentrations from 3 to 10%. The rate of change of velocity and strain rate across the nozzle exhibits plug flow behavior. (D) Extrusion of different nanosilicate concentrations at the same printing settings (scale bar = 10 mm). The extrusion pictures validate the results of the CFD profiles of velocity and strain rate. (E) CFD profiles of pressure in the nozzle for different nanosilicate concentrations. The results show that 6% nanosilicate concentration can be used as a rheological modifier for bioprinting without much damage to cells.

showing thixotropy. This means that extruded nanosilicate formulations can be reused for extrusion-based 3D printing applications, if desired. For a single cycle peak hold test, the first stage was subjected to low shear (0.1 s^{-1} for 60 s), the second stage was subjected to high shear (3000 s^{-1} for 5 s), and the third stage was again subjected to low shear (0.1 s^{-1} for 180 s). The recovery of extrudate is an important factor to consider for direct ink writing. The rebuilding or increase in viscosity after releasing the applied force is also termed as thixotropy. We considered 80% viscosity recovery as significant [17], and we calculated the recovery time by taking the initial viscosity as the maximum viscosity (100% viscosity). Concentrations from 1% to 3% did not show recovery to 80% of the initial viscosity even after 180 s and, hence, did not show good thixotropic behavior (Fig. 2B). Concentrations above 4% showed thixotropy by rebuilding the internal structure. In particular, 4% showed a time of about 35 s to recover the viscosity, whereas 5% showed a time of about 15 s to recover (Fig. 2B, table). Concentrations from 6% and above showed a recovery time of about 7 s, which can be considered as fast recovery time for extrusion-based 3D printing of soft materials. Also, it is worth noting that all concentrations from 4% and above regained 100% of the initial viscosity after adequate time.

Computational fluid dynamics (CFD) simulations were performed on different concentrations of nanosilicates in ANSYS Fluent. The values

obtained from the rotational shear rate sweep by applying the power law were input in the software. The inlet speed and minimum and maximum viscosity from the shear rate range were input in the software and simulations were performed. The simulations were performed on the nozzles' opening since that is the area that is susceptible to most change in velocity and strain rate due to the change in cross-sectional area of the needle. The results of the simulations (Fig. 2C and Fig. S3) show that with increase in nanosilicate concentration, the gradient in the velocities and strain rates become lower from the center to the wall across the nozzle opening. This indicates that a higher concentration of nanosilicates leads to plug flow behavior and the ink moves as viscoelastic solid while exiting the extruder tip. This can be good for cell shielding as long as the extrusion pressure is below the pressure detrimental to cell survival.

Different concentrations from 3% to 10% were extruded by keeping the nozzle tip 30 cm from the printer bed to assess the quality of the extrudate. The extrusion tests using the 3D printer (Fig. 2D) revealed that 2%, 3% and 4% concentrations were not able to print long continuous strands. In contrast, concentrations of 5% and above formed long continuous strands, which makes them favorable for 3D printing. Also, it can be seen in Fig. 2D that 3% nanosilicate solution extruded like droplets of water and formed a pool of ink, whereas higher concentrations formed filaments. These tests also validated the results from CFD simulations that concentrations of 4% and above behave like a viscoelastic solid with a plug flow behavior. We also performed CFD simulations to find the pressure in the nozzle for various nanosilicate concentrations (Fig. 2E). The results showed that maximum pressure was around 0.1 MPa in 10% concentration and the minimum pressure was around 7 kPa in 4% and lower concentrations. The maximum pressure for 6% concentration was around 30 kPa. This is very low pressure to cause cell damage and mammalian cells remain viable at this pressure [48,49]. This shows that nanosilicate can be used with cells as a bioink for making tissue engineered grafts.

3.3. *Extrusion-based 3D printing of nanosilicate*

Simple line structures were printed using nanosilicates concentrations between 3% and 10% w/v to measure the precision of the printed structures compared to the computer-generated design. To quantify the precision, the width, area and volume values of the prints were normalized to that of the computer-generated design. From the extrusion of a simple line, the normalized values showed that pooling of ink occurred in the 3% and 4% formulations, as their normalized values in all three dimensions were more than 100 (Fig. 3A). Thus, these

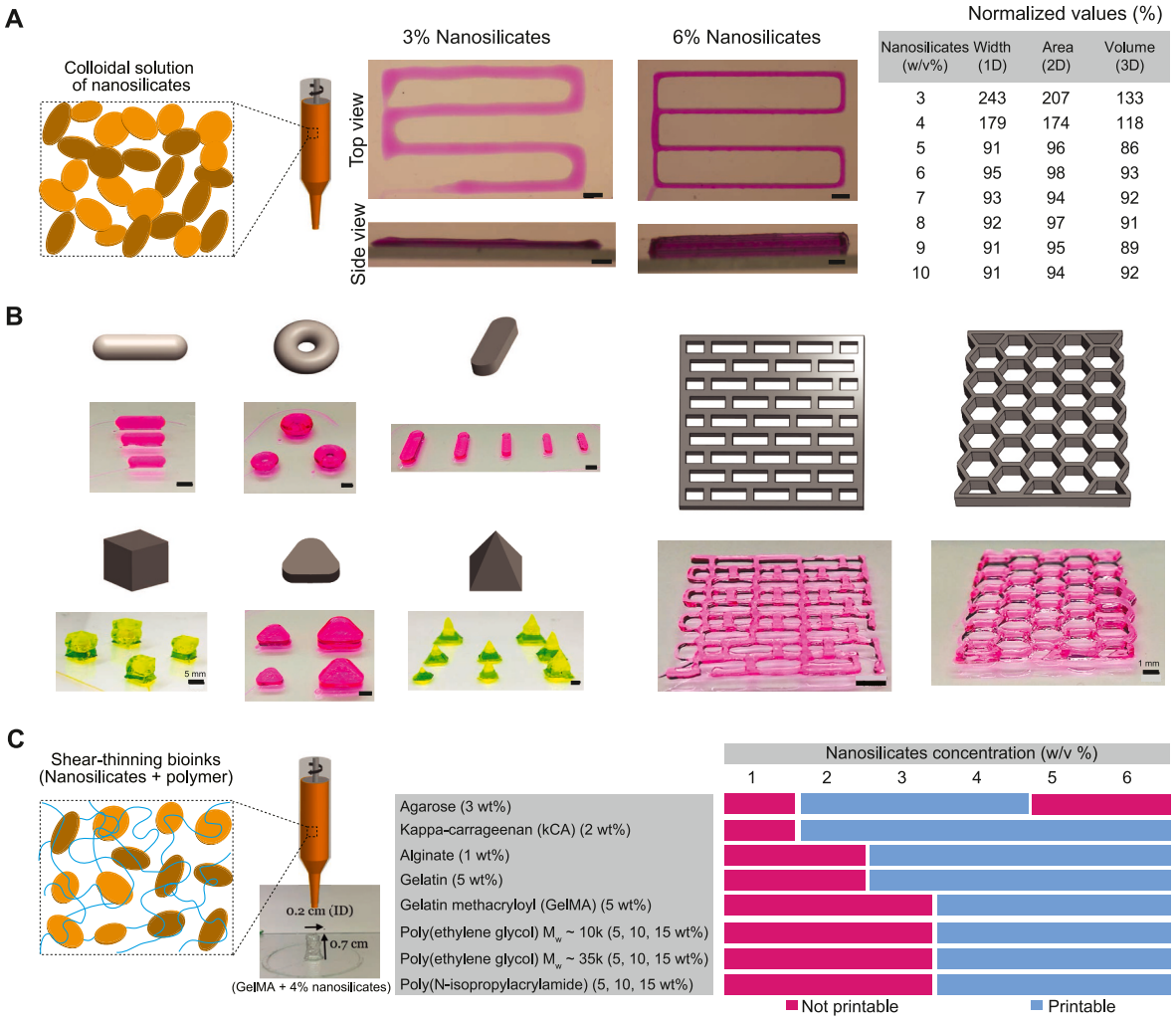

Fig. 3. 3D extrusion printing of nanosilicate and nanosilicate-based inks. (A) 3D printed line structure for 3% and 6% nanosilicate to calculate the shape fidelity values (scale bar = 2 mm). The table shows the shape fidelity values normalized to the computer aided design (CAD) for width, area and volume. (B) CAD file and 3D printed structures of different shapes and sizes using 6% nanosilicate as the ink (scale bar = 5 mm for non-grid structures and 1 mm for grid structures) forming self-supporting structures (C) 3D printability of nanosilicate-polymer composite is shown for selected polymer. Pink color represents not printable formulation, while blue represent printable formulation. This shows the versatility of nanosilicate that can be used with a variety of water-soluble polymers for various applications. (For interpretation of the references to color in this figure legend, the reader is referred to the Web version of this article.)

concentrations did not hold their shape after extrusion and spread widely upon extrusion. Normalized values for concentrations of 5% and above showed that the strands did not spread more than CAD design and held water in its place, as the normalized values were lower than 100 (Fig. 3A, table). Hence, concentrations from 5% and above were deemed suitable for 3D printing. Since 6% had the best normalized values that were near 100, it was deemed to be the better concentration to 3D print structures. It is also worth noting that higher concentrations showed lower normalized values compared to 6%. We believe that this result can be attributed to the higher interaction and packing density between the nanodiscs in the formulation. Concentrations higher than 6% would probably require higher pressure to be extruded to have the same extrusion width.

With the same printing parameters described earlier and 6% nanosilicate, complex structures of different shapes and sizes were printed. The printed structures held their shaped very well, and the 3D prints had good shape fidelity (Fig. 3B). The prints were very smooth, precise and they self-supported their own weight. Although the structures were printed very precisely, the structures lacked rigidity since they were just gels.

Long-term rigidity and robust mechanical properties can be imparted to the structures by adding different types of water-based polymers in the formulation, printing, and crosslinking the structures. To demonstrate this approach, nanosilicate was mixed with various water-soluble polymers (agarose, alginate, kappa-carrageenan (kCA), gelatin, gelatin methacryloyl (GelMA), poly(ethylene glycol) (PEG), and N-isopropylacrylamide (NIPAM)) to obtain hydrogel ink. The printable ink formulation was determined by printing structures with good shape fidelity (Fig. 3C). These results demonstrate that nanoengineered inks obtained by combining nanosilicate and polymers can be used to print constructs for 3D printing application.

3.4. Nanosilicate for drug delivery applications

Drug release from nanosilicate was demonstrated by 3D printing grid structures with 6% nanosilicate loaded with different doxorubicin (Dox) concentrations. These grid structures were then exposed to MDA-MB-231 cells (triple negative breast cancer cells or TNBCs) for 24 h to observe the effect of doxorubicin on the cancer cells. It was observed that Dox loading in the nanosilicate caused an inhibition of cell growth near the grid structures, and increasing the Dox concentration increased the zone of inhibition (Figs. 4A and S4). Similarly, we demonstrated a synergistic effect of BMS-777607 (tyrosine kinase inhibitor) and LGK794 (Wnt inhibitor) loaded in nanosilicate to inhibit TNBC cell growth (Fig. 4B). These synergistic inhibitory effects were further validated using Western blots to quantify the relative expression of p21 and cyclinD1 proteins, both of which play a key role in cellular division and growth in breast cancer cells [50,51](Fig. S5). These results show that 3D printed nanosilicate can be used as a drug delivery platform for developing medical devices with controlled drug release profile.

3.5. Nanosilicate as a sacrificial ink for fabrication of hydrogel-based microfluidic devices

After assessing the printing characteristics of different concentrations of Nanosilicates and identifying 6% and above as good concentrations for extrusion-based 3D printing, we wanted to further investigate the use of nanosilicate as a sacrificial ink for making hydrogel-based microfluidic devices. Organ-on-a-chip devices have been explored widely to mimic various physiologies of different tissues and organs [52]. The main advantage of these organ-on-a-chip (microfluidic) devices is the capability to perform 3D cell culture with dynamic flow behavior inside the channels that is not possible with traditional static systems [53]. These can be used for various applications to emulate and study vascular physiology and fluid mechanics, disease models, tissue organization and function, therapeutic tissue engineering, as 3D cell culture models, and to screen drugs [25,54]. Traditionally, polydimethylsiloxane (PDMS) and thermoplastics such as polycarbonate have been used for making these organ-on-a-chip devices, which lack good cytocompatibility and diffusional permeability. As a result, many studies have used hydrogel-based microfluidic devices that have been fabricated using different techniques and methods [55]. However, most of these fabrication techniques require complicated steps, which are difficult to control and are sensitive to employ. The need for more facile strategies led us to investigate the use of nanosilicate as a sacrificial ink for the fabrication of hydrogel-based organ-on-a-chip devices.

For fabricating the hydrogel microfluidic device, we used a

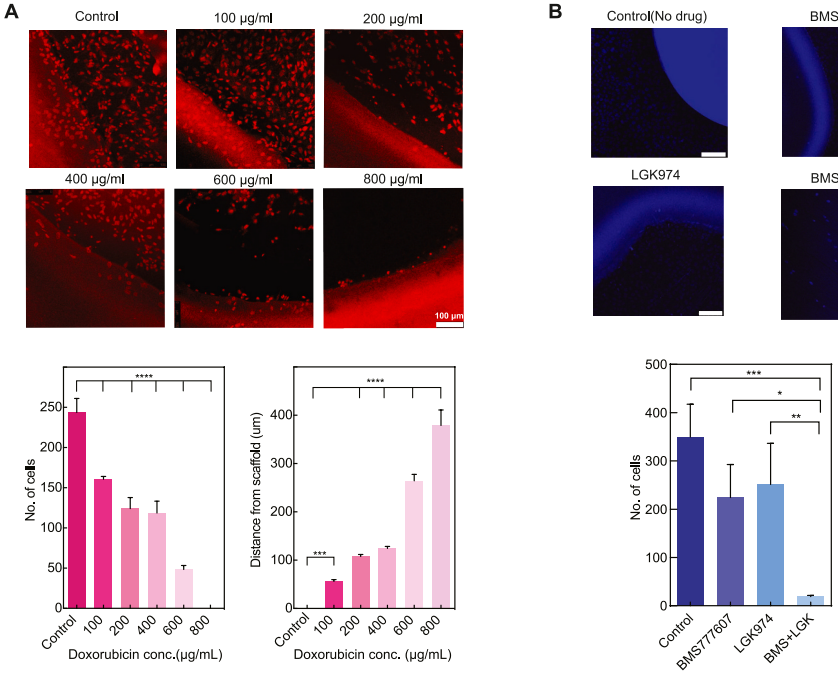

Fig. 4. 3D printed nanosilicate as a drug delivery platform. (A) Fluorescent images of doxorubicin-loaded 3D printed nanosilicate (6% w/v in DI water) exposed to triple negative breast cancer cells at various concentrations. The number of live cells and distance from the scaffold were quantified at the bottom (scale bar = 0.1 mm) showing concentration dependent controlled release of drugs from nanosilicates (B) Synergistic inhibition effect of BMS777607 (tyrosine kinase inhibitor) and LGK974 (Wnt inhibitor) co-delivery on triple negative breast cancer cells (scale bar = 0.1 mm). The inhibition effects of co-delivery are significantly different compared to control and single inhibitor delivery.

combination of 5% w/v Gelatin Methacryloyl (GelMA), 5% w/v Gelatin, and 0.25% w/v Irgacure 2959 as the photoinitiator (hydrogel formulation). This combination has been used to make hydrogel microfluidic devices previously and has shown good bonding strength, optical transparency and cytocompatibility [56]. Both gelatin and Gelatin methacryloyl (GelMA) contain arginine-glycine-aspartic acid (RGD) sequences that aid in cell attachment along with target sequences of matrix metalloproteinase (MMP) that are appropriate for cell remodeling. In addition, this combination of GelMA and gelatin can be used for two-phase crosslinking. Gelatin and GelMA show reversible physical thermal crosslinking (sol gel transition) due to coiling and uncoiling of polymer chains, whereas GelMA can also be chemically crosslinked by using UV light along with a photoinitiator (Irgacure 2959 in this case). Both gelatin and GelMA are cytocompatible as shown by previous studies and can demonstrate physiological stability over extended period of more than 20 days [56,57].

A mixture of 5% w/v GelMA, 5% w/v of Gelatin and 0.25% w/v Irgacure 2959 was added to DI water, stirred for an hour at 50 °C, and used as a hydrogel medium for making the microfluidic channels. For making the devices, this formulation was poured and cast into an acrylic box by keeping it at 4 °C. After that, the formulation solidified due to thermal gelation of both gelatin and GelMA. On top of this solidified layer, 6% w/v Nanosilicates was extruded using the 3D printer in the form of channels. After the nanosilicates were printed, a heated hydrogel formulation was poured on top of the printed layer and kept at 4 °C. This formed a bilayer device that was photocrosslinked using the UV light. Once the top layer was cured, the cured device was taken out of the cast box using a spatula. Then, the device was inverted, and the bottom layer was cured with the UV light. Once both the layers were UV cured, PBS was flushed through the channels to remove the nanosilicates from the channels. We were able to precisely print nanosilicate on top of a natural polymer as both the nanosilicate formulation and hydrogel had high water content and were hydrophilic. We had hypothesized that there would be layer adhesion between nanosilicates and polymer gels due to their hydrophilicity. A schematic of the fabrication process is shown in Fig. 5A.

By using 6% w/v nanosilicate and the process described above, we printed different shapes and sizes of channels. We were able to fabricate channels in the hydrogels using Nanosilicates as a sacrificial ink. We fabricated both straight channels and complex channels inside the cast hydrogel formulation. For complex structures, we were able to make bifurcated channels, multibranched channels, and serpentine channels (Fig. 5B). To show the patency of these channels, we perfused them with fluorescein isothiocyanate (FITC) -labeled microbeads. We were also able to print different sizes of straight channels on the same device. The average sizes of the channels were about 220 μm, 600 μm, 1000 μm and 1200 μm from thinnest to thickest (Fig. S6). These results show that a variety of sizes of channels can be printed and this sacrificial method can be used to print very thin channels by extrusion of nanosilicate.

To test the diffusion permeability of the hydrogels, fluorescein isothiocyanate (FITC) tagged 40 kDa dextran was perfused through a 1200 μm straight channel. Dextran diffusion served as a model for protein diffusion through the hydrogel matrix and mass transfer through the channel. The results showed the diffusion of dextran over time through the hydrogel material (Fig. 5C). Images were processed in ImageJ, and a Look up table (LUT) was applied for enhanced contrast and better visibility of diffusion through the lumen. Diffusion was measured by quantifying the fluorescence intensity inside the channel over 60 min with 10 min time point gaps, and the sinusoidal profile was mapped on a graph (Fig. 5C), which showed a decrease in intensity of dextran through the channel over time. The inset shows the increase in fluorescent intensity outside the channel over 60 min. We also showed perfusion of

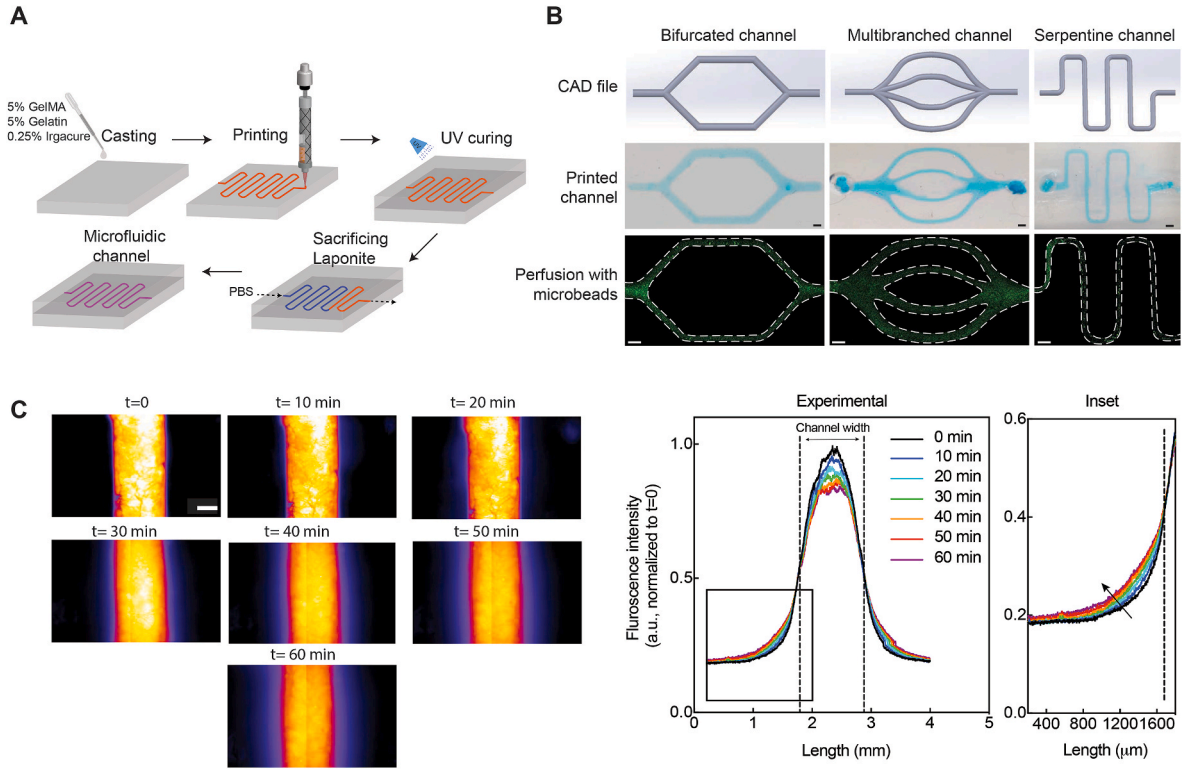

Fig. 5. Nanosilicate as sacrificial ink for fabricating hydrogel-based microfluidics. (A) Schematic showing the process of fabricating the hydrogel based microfluidic devices. (B) Three different designs (bifurcated channel, multibranched channel, and serpentine channel) with their CAD files, 3D printed nanosilicate layer trapped between two hydrogel layers, and perfusion with FITC labeled microbeads (Scale bar = 0.5 mm). This shows that complex channels can be fabricated with this process (C) Time-course study of FITC labeled dextran diffusion through the walls of the channel with fluorescent images (scale bar = 0.5 mm) on the right, graph showing the quantification of diffusion of dextran through the walls of the channel on the left. Inset shows the increase of fluorescent signal outside the channel longitudinally, indicating the mass transfer of model protein (FITC) through the hydrogels.

different dyes through two adjacent straight channels in the same device (Fig. S6). This establishes that these materials and the fabrication process can be used for making a hydrogel-based microfluidic channels in applications that need diffusional permeability through the microfluidic device material. We expect these devices to have good cytocompatibility based on the biocompatible materials used for fabricating these devices.

3.6. Nanosilicate as a sacrificial support bath

There has been a growing increase in the number of research studies on 3D printing of soft materials inside a support bath over the past few years [29]. One of the main advantages of this type of printing process is that gravitational and surface tension properties that negatively affect 3D printing in air are nullified by printing inside the support bath. This has led researchers to investigate various biomaterials for both the sacrificial support bath (also termed as embedded 3D printing/suspension bath printing) and ink for 3D printing and bioprinting [58]. In this 3D printing method, a gel-like medium supports another fluidic material (or ink) which is extruded inside the gel-like medium. The extruded material is crosslinked using a suitable methodology after the printing process has been completed. The support material/gel-like medium is usually sacrificed or removed to extract the crosslinked solidified printed structure. This 3D printing process requires the support material to remain a gel when no shear force is applied. However, it should behave as a liquid/fluid when a shear force is applied and then again become a gel when the shear force is removed. The shearing of the fluid in this case is caused by the translation of the nozzle inside the support bath that dispenses the ink. Hence, the support bath material should be a viscoelastic fluid that has good shear thinning and thixotropic properties. Various natural and synthetic materials have been explored as support bath materials in different studies [58,59]. Interfacial forces limit the use of this 3D printing technique to inks and support baths that have same the dispersion medium, ie, hydrophilic ink should be used in a hydrophilic support bath and hydrophobic inks should be used in hydrophobic support bath [60]. Some of the most common materials that have been used as support bath materials include blends of polyacrylic acid, gelatin microparticles and colloidal platelets. All these materials have their distinct advantages and disadvantages over one another, depending on the application of the printing.

Apart from appropriate rheological properties required for a support bath, the combination of both inks and support bath should have suitable rheological properties at the same time [61]. Generally, the shear elastic modulus and yield stress of the support bath, G'support and $\tau_{y,}$ support, should be one order of magnitude lower than the corresponding values for the ink, G'_{ink} and $\tau_{y,ink,}$ respectively. If G'support is too high compared to G'_{ink}, the ink would be discontinuous and form beads inside the support bath. In contrast, if G'support is too low compared to G'_{ink}, the ink would be extruded improperly and would drag inside the support bath. In addition, the yield stress of the support bath, $\tau_{y,}$ support should not be too low or too high compared to the shear forces applied by the translation of the nozzle inside the support bath. If $\tau_{y,}$ support is too low, the forces created by the translating nozzle would affect and displace the printed features. Conversely, if $\tau_{y,}$ support is too high, the translating nozzle would create crevasses in its wake that would not be conducive to printing inside a support bath. These forces are also affected by other factors such as the translating speed of the nozzle and flow rate of the ink.

As nanosilicates exhibit the rheological properties suitable for a support bath material such as shear thinning, yield stress and thixotropic behavior, we investigated their use as a sacrificial support bath for 3D printing. In support bath printing, initially, the "house-of-cards" structure is present across the nanosilicate formulation. As the nozzle translates inside the nanosilicate support bath during printing, the "house-of-cards" structure is broken down in the area close to nozzle translation and the nanosilicate in the needle's path is displaced. Once the nozzle passes a particular place in its path, the displaced nanosilicate restructures due to its thixotropic behavior and traps the ink material extruded by the needle. We used a combination of gelatin methacryloyl (GelMA) and Kappa-carageenan (κCa) with Irgacure 2959 as the photointiator, for printing inside the nanosilicate support bath. We selected GelMA for its good biocompatibility. κCa was used to enhance the flow properties of GelMA at room temperature. κCa is a linear sulfated polysaccharide with alternating β-D-galactose-4-sulphate and 3,6-anhydro-D-galactose sourced from red algae.

We investigated different concentrations of Nanosilicates and ink proportions to get an optimal working system for the 3D printing process. The concentration of GelMA was set at 10% w/v while we tried three concentrations of κCa, 1.0%, 0.9%, and 0.8% w/v. The higher κCa concentrations of 1% and 0.9% proved difficult to be extruded for the printing conditions, but 0.8% showed good extrudability and, hence, it was chosen for the ink formulation. We assessed concentrations of 3% (w/v) and higher of Nanosilicates for the support bath as only they showed a formation of house of cards and had a yield stress, as shown before. When 3% nanosilicate was used, the area near the translating nozzle would fluidize but did not restructure fast enough to support the printed structure. This led to dragging of the ink inside the support bath. This was likely due to the G'_{ink} being high compared to G'support and due to the slow thixotropic response of the support bath. Concentrations of 5% and above formed a crevasse in the wake of nozzle translation, which was an impediment to printing inside the support bath. This can be attributed to the high yield stress of these concentrations.

Based on these results, we chose 4% w/v Nanosilicates as the support bath for 3D printing the selected ink formulation. A schematic of the support bath printing process is shown in Fig. 6A. The ink was mixed with FITC/rhodamine to provide better visibility to the otherwise translucent ink. The same extrusion-based printer as described before was used for printing in the support bath. The XY speed of the printer head was kept at 2 mm/s. Different designs such as a square, Y shaped bifurcated vessels, a curved bifurcated vessel, a small-scale human femur, pancreas, and meniscus were printed inside the support bath (Fig. 6B, S7, and S8). We were also able to print other complex structures, such as the structure of DNA, a small-scale human heart and trileaflet valve inside the support bath. After the structures were printed, they were exposed to UV light at an intensity of about 30 mW/cm^2 for photo-crosslinking inside the bath. The printed structures were extracted out of the support bath by diluting the support bath with DI water/PBS. Then, they were kept in a 5% w/v Potassium Chloride (KCl) solution for 30 min for physical crosslinking of κCa. The extracted printed structures were comparable in dimensions to the software designs (Fig. 6C).

We performed mechanical tests on printed cylindrical constructs and compared them with cast constructs made of same hydrogel formulation to test for differences resulting from the printing process. Unconfined uniaxial compression was performed on the cylindrical constructs to 30% compression, and the stress-strain profiles were plotted. The stress-strain curves of both printed and cast structures were similar (Fig. 7A). Compressive modulus, toughness and maximum stress were derived from the strain-strain curves. For printed constructs, the values for compression modulus were 44.32 ± 3.03 kPa, toughness were 2.42 ± 0.27 kJ/m^3 and, maximum stress at maximum strain were 22.47 ± 1.67 kPa. For cast constructs, the values for compression modulus were 50.13 ± 7.14 kPa, toughness were 2.74 ± 0.40 kJ/m^3 and, maximum stress at maximum strain were 28.69 ± 4.85 kPa. There was no significant difference between the different values between cast and printed constructs.

Scanning electron microscopy (SEM) micrographs of the cross sections of both printed and cast samples were also compared to visualize the interconnected porosity. Similar porosity was observed for both the samples (Fig. 7B). Additionally, we performed Energy Dispersive X-Ray Spectroscopy (EDX or EDS) on samples to verify the presence of nanosilicate in the printed samples. The presence of Magnesium (Mg) and Silicon (Si) indicated that nanosilicate was present inside the constructs,

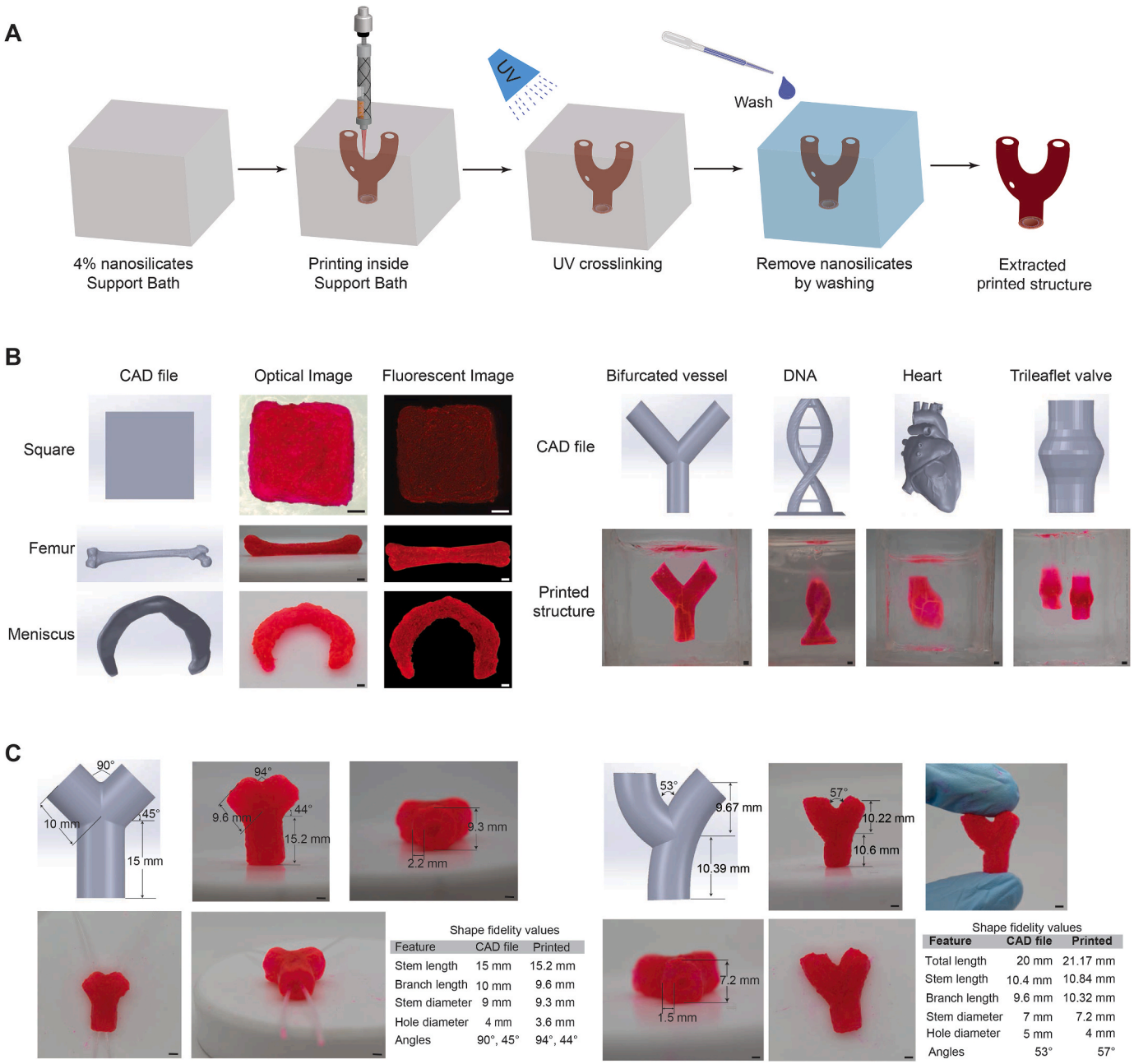

Fig. 6. Nanosilicate as sacrificial support bath for support bath 3D printing. (A) Schematic of nanosilicate support bath 3D printing process -. (B) Computer aided design (CAD) file, optical image and fluorescent image of various 3D printed structures (square, small scaled anatomical human femur, meniscus, vertical Y shaped bifurcated vessel, DNA structure, small scaled human anatomical heart and trileaflet valve) extracted from the nanosilicate support bath (Scale bar = 2 mm). (C) CAD files, optical images and shape fidelity values of structures printed in the support bath - straight bifurcated vessel and curved bifurcated vessel (Scale bar = 2 mm). This demonstrates that tall, complex structures with good shape fidelity can be 3D printed inside the nanoclay support bath.

likely due to diffusion or entrapment of nanosilicate particles between the layers of ink during the printing process. However, the presence of nanosilicate could be advantageous for bone, cartilage or vascular tissue engineering applications, as previous studies have shown that nanosilicate promotes bone [62,63] and cartilage [64] regeneration, and angiogenesis [65].

To investigate the cytocompatibility of our constructs and printing process, we performed two-dimensional (2D) cell seeding of human umbilical vein endothelial cells (HUVECs) on the printed and cast cylindrical constructs. GelMA is already a widely used cytocompatible material, and the GelMA/κCa combination has already been shown to be cytocompatible for various cell types [22,57,66]. We chose to use HUVECs since they are one of the most widely studied human cell lines and endothelial cells are present throughout our body. We conducted the study for 7 days and found that HUVECs were viable and spread well on the surface of the printed construct. Actin and nuclei staining showed the presence of cells on the surface for all 7 days (Fig. 7C). We also performed the Alamar Blue assay on printed and cast constructs to quantify cell viability. Although the overall cell viability decreased for both constructs, there was no significant difference between the two groups for 7 days (Fig. 7D). Additionally, the cell viability remained above 75% for the printed construct for the entire 7 days. We believe the reason for low proliferation of HUVECs over 7 days is the high modulus of our hydrogel matrix since the cell viability was lower for both cast and 3D printed formulations. This can be overcome by lowering the stiffness of the crosslinked hydrogels by reducing the intensity of the UV light or

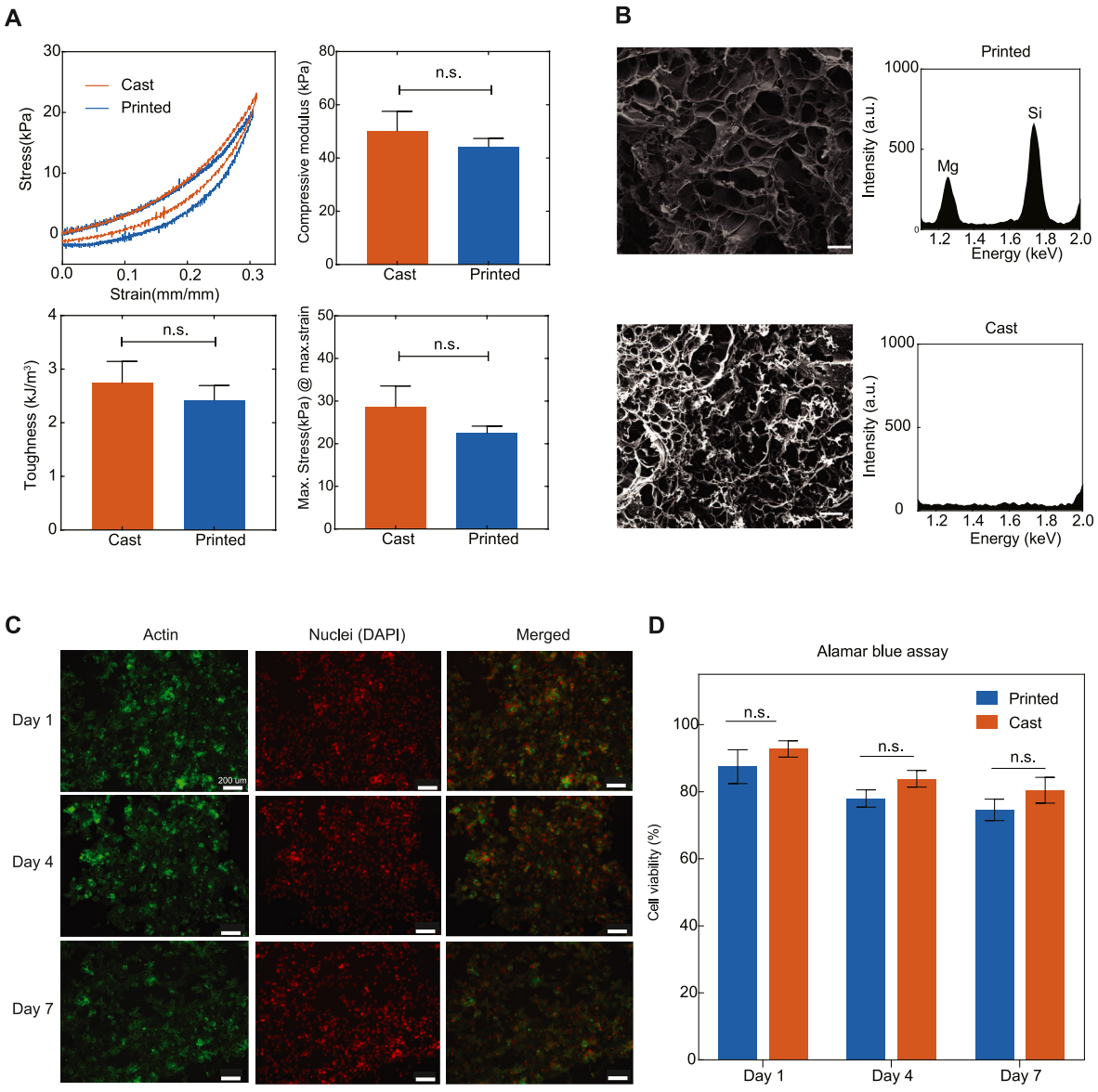

Fig. 7. Mechanical, structural and cell viability comparison of cast hydrogels and support bath 3D printed hydrogels. (A) Stress-strain profiles; comparison of compressive modulus, toughness, and maximum stress at maximum strain of cast and support bath 3D printed cylindrical structures. There is no significant difference in mechanical properties of cast and 3D printed constructs. (B) Scanning electron microscopy (SEM) images (Scale bar = 50 μ m) and Energy-dispersive X-ray spectroscopy (EDS) spectra of support bath 3D printed and cast structures. The morphological structures of cast and 3D printed constructs are similar with the 3D printed constructs embedded with nanosilicates. (C) Actin (Phallodin) and nuclei (DAPI) stained images for HUVEC cells seeded on 3D support bath printed hydrogel constructs (10% w/v GelMA + 0.8% κCa) for 1, 4 and 7 days (Scale bar = 200 μm). (D) Cell viability of HUVECs calculated on 3D support bath printed constructs (using Alamar Blue assay) for 1, 4 and 7 days exhibiting cytocompatibility of 3D printed hydrogels.

by reducing the UV exposure time for crosslinking the hydrogels. Although, we used a GelMA and κCa based ink for printing inside the nanosilicate support bath, other hydrogels/soft materials can be used as ink for printing inside the nanosilicate support bath [67].

4. Conclusion

In this study, we established the use of nanosilicate as a platform technology for soft matter additive manufacturing applications. First, we characterized different concentrations of nanosilicate using both qualitative and quantitative (rheological) characterization techniques. Then, we 3D printed different structures of various shapes and sizes using 6% w/v nanosilicate. We also reinforced different polymeric hydrogels with nanosilicates and render them printable, demonstrating the ability of nanosilicate as rheological additive to fabricate biomaterials-based inks for 3D printing or bioprinting. Next, we used nanosilicate as a sacrificial ink to make hydrogel-based microfluidic devices. We showed that different shape and size channels could be easily printed for making microfluidic devices. We also showed perfusion through these channels. These devices can be used for modelling physiological conditions and diseases and are superior to conventional organ-on-a-chip devices (PDMS/Polycarbonate/Acrylic based) because they allow easy diffusion through the channels, which can better mimic actual physiological conditions. In addition, we showed that nanosilicate can also be used as a sacrificial support bath for printing complex structures. This was done by printing different structures such as bifurcated vessels, femur, meniscus, DNA double helix, heart, and tri-leaflet valve inside the support bath. Future studies will further investigate the biocompatibility of the systems and methods developed in this study. Hence, through this study we established the versatility of

nanosilicates as an additive for water-based formulations for extrusion-based additive manufacturing, sacrificial ink for fabrication of hydrogel based microfluidic devices, and as support bath additive manufacturing. The versatility of nanosilicate-based biomaterials can be applied to the fields of soft matter additive manufacturing, tissue engineering, and medical devices.

CRediT authorship contribution statement

Satyam Rajput: Conceptualization, Data curation, Formal analysis, Writing – original draft.

Kaivalya A. Deo: Data curation, Formal analysis, Writing – review & editing.

Tanmay Mathur: Data curation, Formal analysis.

Giriraj Lokhande: Data curation, Formal analysis.

Kanwar Abhay Singh: Data curation, Formal analysis.

Yuxiang Sun: Data curation, Formal analysis.

Daniel L. Alge: Data curation, Formal analysis.

Abhishek Jain: Data curation, Formal analysis.

Tapasree Roy Sarkar: Data curation, Formal analysis.

Akhilesh K. Gaharwar: Conceptualization, Formal analysis, Writing – original draft, Writing – review & editing.

Declaration of competing interest

The authors declare that they have no known competing financial interests or personal relationships that could have appeared to influence the work reported in this paper.

Acknowledgements

A.K.G. would like to acknowledge financial support from the National Institute of Biomedical Imaging and Bioengineering (NIBIB) of the National Institutes of Health (NIH) Director's New Innovator Award (DP2 EB026265), the National Science Foundation (NSF) Award (CBET 1705852). A.K.G., A.J., Y.S. and D.A. would like to thank the President's Excellence Fund (X-Grants & T3) from Texas A&M University. The content is solely the responsibility of the authors and does not necessarily represent the official views of the funding agency. We would like to thank Almira Rajwani and Raul Martinez for their assistance in this work.

Appendix A. Supplementary data

Supplementary data to this article can be found online at https://doi.org/10.1016/j.bprint.2021.e00187.

References

[1] Y.S. Zhang, R. Oklu, M.R. Dokmeci, A. Khademhosseini, Three-dimensional bioprinting strategies for tissue engineering, Cold Spring Harb Perspect Med 8 (2) (2018).
[2] R.L. Truby, J.A. Lewis, Printing soft matter in three dimensions, Nature 540 (2016) 371.
[3] K.A. Deo, K.A. Singh, C.W. Peak, D.L. Alge, A.K. Gaharwar, Bioprinting 101: design, fabrication, and evaluation of cell-laden 3D bioprinted scaffolds, Tissue Eng. 26 (5–6) (2020) 318–338.
[4] D. Chimene, R. Kaunas, A.K. Gaharwar, Hydrogel bioink reinforcement for additive manufacturing: a focused review of emerging strategies, Adv. Mater. 32 (1) (2020) 1902026.
[5] Y.S. Zhang, G. Haghiashtiani, T. Hübscher, D.J. Kelly, J.M. Lee, M. Lutolf, M. C. McAlpine, W.Y. Yeong, M. Zenobi-Wong, J. Malda, 3D extrusion bioprinting, Nature Reviews Methods Primers 1 (1) (2021) 75.
[6] X. Li, H. Wang, D. Li, S. Long, G. Zhang, Z. Wu, Dual ionically cross-linked double-network hydrogels with high strength, toughness, swelling resistance, and improved 3D printing processability, ACS Appl. Mater. Interfaces 10 (37) (2018) 31198–31207.
[7] Q. Gao, X. Niu, L. Shao, L. Zhou, Z. Lin, A. Sun, J. Fu, Z. Chen, J. Hu, Y. Liu, Y. He, 3D printing of complex GelMA-based scaffolds with nanoclay, Biofabrication 11 (3) (2019), 035006.
[8] R. Schipani, S. Scheurer, R. Florentin, S.E. Critchley, D.J. Kelly, Reinforcing Interpenetrating Network Hydrogels with 3D Printed Polymer Networks to Engineer Cartilage Mimetic Composites, Biofabrication, 2020, 035011.
[9] S.A. Wilson, L.M. Cross, C.W. Peak, A.K. Gaharwar, Shear-thinning and thermo-reversible nanoengineered inks for 3D bioprinting, ACS Appl. Mater. Interfaces 9 (50) (2017) 43449–43458.
[10] T.J. Tigner, S. Rajput, A.K. Gaharwar, D.L. Alge, Comparison of photo cross linkable gelatin derivatives and initiators for three-dimensional extrusion bioprinting, Biomacromolecules 21 (2) (2020) 454–463.
[11] K.W.M. Boere, M.M. Blokzijl, J. Visser, J.E.A. Linssen, J. Malda, W.E. Hennink, T. Vermonden, Biofabrication of reinforced 3D-scaffolds using two-component hydrogels, J. Mater. Chem. B 3 (46) (2015) 9067–9078.
[12] S. Kyle, Z.M. Jessop, A. Al-Sabah, I.S. Whitaker, 'Printability' of candidate biomaterials for extrusion based 3D printing: state-of-the-art, Advanced Healthcare Materials 6 (16) (2017) 1700264.
[13] S. Hong, D. Sycks, H.F. Chan, S. Lin, G.P. Lopez, F. Guilak, K.W. Leong, X. Zhao, 3D printing of highly stretchable and tough hydrogels into complex, cellularized structures, Adv. Mater. 27 (27) (2015) 4035–4040.
[14] A.K. Gaharwar, L.M. Cross, C.W. Peak, K. Gold, J.K. Carrow, A. Brokesh, K. A. Singh, 2D nanoclay for biomedical applications: regenerative medicine, therapeutic delivery, and additive manufacturing, Adv. Mater. 31 (23) (2019) 1900332.
[15] Mourchid, A. Mourchid, A. Delville, J. Lambard, E. LeColier, P. Levitz, Phase diagram of colloidal dispersions of anisotropic charged particles: equilibrium properties, structure, and rheology of laponite suspensions, Langmuir 11 (6) (1995) 1942–1950.
[16] B. Ruzicka, E. Zaccarelli, A fresh look at the Laponite phase diagram, Soft Matter 7 (4) (2011) 1268–1286.
[17] C.W. Peak, J. Stein, K.A. Gold, A.K. Gaharwar, Nanoengineered colloidal inks for 3D bioprinting, Langmuir 34 (3) (2018) 917–925.
[18] Y. Jin, C. Liu, W. Chai, A. Compaan, Y. Huang, Self-supporting nanoclay as internal scaffold material for direct printing of soft hydrogel composite structures in air, ACS Appl. Mater. Interfaces 9 (20) (2017) 17456–17465.
[19] G. Cidonio, C.R. Alcala-Orozco, K.S. Lim, M. Glinka, I. Mutreja, Y.-H. Kim, J. I. Dawson, T.B.F. Woodfield, R.O.C. Oreffo, Osteogenic and angiogenic tissue formation in high fidelity nanocomposite Laponite-gelatin bioinks, Biofabrication 11 (3) (2019), 035027.
[20] A. Motealleh, B. Çelebi-Saltik, N. Ermis, S. Nowak, A. Khademhosseini, N.S. Kehr, 3D printing of step-gradient nanocomposite hydrogels for controlled cell migration, Biofabrication 11 (4) (2019), 045015.
[21] T. Ahlfeld, G. Cidonio, D. Kilian, S. Duin, A.R. Akkineni, J.I. Dawson, S. Yang, A. Lode, R.O.C. Oreffo, M. Gelinsky, Development of a clay based bioink for 3D cell printing for skeletal application, Biofabrication 9 (3) (2017), 034103.
[22] D. Chimene, L. Miller, L.M. Cross, M.K. Jaiswal, I. Singh, A.K. Gaharwar, Nanoengineered osteoinductive bioink for 3D bioprinting bone tissue, ACS Appl. Mater. Interfaces 12 (14) (2020) 15976–15988.
[23] K. Gold, A.K. Gaharwar, A. Jain, Emerging trends in multiscale modeling of vascular pathophysiology: organ-on-a-chip and 3D printing, Biomaterials 196 (2019) 2–17.
[24] E.K. Sackmann, A.L. Fulton, D.J. Beebe, The present and future role of microfluidics in biomedical research, Nature 507 (2014) 181.
[25] S. Fleischer, D.N. Tavakol, G. Vunjak-Novakovic, From arteries to capillaries: approaches to engineering human vasculature, Adv. Funct. Mater. 30 (37) (2020) 1910811.
[26] M.W. Laschke, Y. Harder, M. Amon, I. Martin, J. Farhadi, A. Ring, N. Torio-Padron, R. Schramm, M. Rücker, D. Junker, J.M. Häufel, C. Carvalho, M. Heberer, G. Germann, B. Vollmar, M.D. Menger, Angiogenesis in tissue engineering: breathing life into constructed tissue substitutes, Tissue Eng. 12 (8) (2006) 2093–2104.
[27] F. Cheng, X. Cao, H. Li, T. Liu, X. Xie, D. Huang, S. Maharjan, H.P. Bei, A. Gómez, J. Li, H. Zhan, H. Shen, S. Liu, J. He, Y.S. Zhang, Generation of cost-effective paper-based tissue models through matrix-assisted sacrificial 3D printing, Nano Lett. 19 (6) (2019) 3603–3611.
[28] I.S. Kinstlinger, J.S. Miller, 3D-printed fluidic networks as vasculature for engineered tissue, Lab Chip 16 (11) (2016) 2025–2043.
[29] A. McCormack, C.B. Highley, N.R. Leslie, F.P.W. Melchels, 3D printing in suspension baths: keeping the promises of bioprinting afloat, Trends Biotechnol. 38 (6) (2020) 584–593.
[30] C.S. O'Bryan, T. Bhattacharjee, S.R. Niemi, S. Balachandar, N. Baldwin, S. T. Ellison, C.R. Taylor, W.G. Sawyer, T.E. Angelini, Three-dimensional printing with sacrificial materials for soft matter manufacturing, MRS Bull. 42 (8) (2017) 571–577.
[31] M. Rocca, A. Fragasso, W. Liu, M.A. Heinrich, Y.S. Zhang, Embedded multimaterial extrusion bioprinting, SLAS TECHNOLOGY: Translating Life Sciences Innovation 23 (2) (2017) 154–163.
[32] T.J. Hinton, Q. Jallerat, R.N. Palchesko, J.H. Park, M.S. Grodzicki, H.-J. Shue, M. H. Ramadan, A.R. Hudson, A.W. Feinberg, Three-dimensional printing of complex biological structures by freeform reversible embedding of suspended hydrogels, Sci. Adv. 1 (9) (2015), e1500758.
[33] T. Bhattacharjee, S.M. Zehnder, K.G. Rowe, S. Jain, R.M. Nixon, W.G. Sawyer, T. E. Angelini, Writing in the granular gel medium, Sci. Adv. 1 (8) (2015), e1500655.
[34] A.M. Compaan, K. Song, Y. Huang, Gellan fluid gel as a versatile support bath material for fluid extrusion bioprinting, ACS Appl. Mater. Interfaces 11 (6) (2019) 5714–5726.
[35] D. Loessner, C. Meinert, E. Kaemmerer, L.C. Martine, K. Yue, P.A. Levett, T.J. Klein, F.P.W. Melchels, A. Khademhosseini, D.W. Hutmacher, Functionalization,

preparation and use of cell-laden gelatin methacryloyl–based hydrogels as modular tissue culture platforms, Nat. Protoc. 11 (2016) 727.
[36] E. Hoch, C. Schuh, T. Hirth, G.E.M. Tovar, K. Borchers, Stiff gelatin hydrogels can be photo-chemically synthesized from low viscous gelatin solutions using molecularly functionalized gelatin with a high degree of methacrylation, J. Mater. Sci. Mater. Med. 23 (11) (2012) 2607–2617.
[37] T.-H. Weng, M.-Y. Yao, X.-M. Xu, C.-Y. Hu, S.-H. Yao, Y.-Z. Liu, Z.-G. Wu, T.-M. Tang, P.-F. Fu, M.-H. Wang, H.-P. Yao, RON and MET Co-overexpression are significant pathological characteristics of poor survival and therapeutic targets of tyrosine kinase inhibitors in triple-negative breast cancer, Cancer Res Treat 52 (3) (2020) 973–986.
[38] J. Liu, S. Pan, M.H. Hsieh, N. Ng, F. Sun, T. Wang, S. Kasibhatla, A.G. Schuller, A. G. Li, D. Cheng, J. Li, C. Tompkins, A. Pferdekamper, A. Steffy, J. Cheng, C. Kowal, V. Phung, G. Guo, Y. Wang, M.P. Graham, S. Flynn, J.C. Brenner, C. Li, M. C. Villarroel, P.G. Schultz, X. Wu, P. McNamara, W.R. Sellers, L. Petruzzelli, A. L. Boral, H.M. Seidel, M.E. McLaughlin, J. Che, T.E. Carey, G. Vanasse, J.L. Harris, Targeting wnt-driven cancer through the inhibition of porcupine by LGK974, Proc. Natl. Acad. Sci. Unit. States Am. 110 (50) (2013) 20224.
[39] R. Torka, K. Pénzes, S. Gusenbauer, C. Baumann, I. Szabadkai, L. Őrfi, G. Kéri, A. Ullrich, Activation of HER3 interferes with antitumor effects of axl receptor tyrosine kinase inhibitors: suggestion of combination therapy, Neoplasia 16 (4) (2014) 301–318.
[40] Y. Matsuda, T. Schlange, E.J. Oakeley, A. Boulay, N.E. Hynes, WNT signaling enhances breast cancer cell motility and blockade of the WNT pathway by sFRP1 suppresses MDA-MB-231 xenograft growth, Breast Cancer Res. 11 (3) (2009) R32.
[41] F. Shao, H. Sun, C.-X. Deng, Potential therapeutic targets of triple-negative breast cancer based on its intrinsic subtype, Oncotarget 8 (42) (2017).
[42] M. Law, E. Forrester, A. Chytil, P. Corsino, G. Green, B. Davis, T. Rowe, B. Law, Rapamycin disrupts cyclin/cyclin-dependent kinase/p21/proliferating cell nuclear antigen complexes and cyclin D1 reverses rapamycin action by stabilizing these complexes, Cancer Res. 66 (2) (2006) 1070.
[43] R. Angelini, E. Zaccarelli, F.A. de Melo Marques, M. Sztucki, A. Fluerasu, G. Ruocco, B. Ruzicka, Glass–glass transition during aging of a colloidal clay, Nat. Commun. 5 (1) (2014) 4049.
[44] B. Ruzicka, E. Zaccarelli, L. Zulian, R. Angelini, M. Sztucki, A. Moussaïd, T. Narayanan, F. Sciortino, Observation of empty liquids and equilibrium gels in a colloidal clay, Nat. Mater. 10 (1) (2011) 56–60.
[45] V. Gupta, M.A. Hampton, J.R. Stokes, A.V. Nguyen, J.D. Miller, Particle interactions in kaolinite suspensions and corresponding aggregate structures, J. Colloid Interface Sci. 359 (1) (2011) 95–103.
[46] A. Shahin, Y.M. Joshi, Hyper-Aging dynamics of nanoclay suspension, Langmuir 28 (13) (2012) 5826–5833.
[47] G. Lagaly, Principles of flow of kaolin and bentonite dispersions, Appl. Clay Sci. 4 (2) (1989) 105–123.
[48] B. Frey, S. Franz, A. Sheriff, A. Korn, G. Bluemelhuber, U.S. Gaipl, R.E. Voll, R. Meyer-Pittroff, M. Herrmann, Hydrostatic pressure induced death of mammalian cells engages pathways related to apoptosis or necrosis, Cell. Mol. Biol. 50 (4) (2004) 459–467.
[49] L. Valon, R. Levayer, Dying under pressure: cellular characterisation and in vivo functions of cell death induced by compaction, Biol. Cell. 111 (3) (2019) 51–66.
[50] S. Ma, J. Tang, J. Feng, Y. Xu, X. Yu, Q. Deng, Y. Lu, Induction of p21 by p65 in p53 null cells treated with Doxorubicin, Biochim. Biophys. Acta 1783 (5) (2008) 935–940.
[51] E. Tarasewicz, R. Hamdan, J. Straehla, A. Hardy, O. Nunez, S. Zelivianski, D. Dokic, J.S. Jeruss, CDK4 inhibition and doxorubicin mediate breast cancer cell apoptosis through Smad 3 and survivin, Cancer Biol. Ther. 15 (10) (2014) 1301–1311.
[52] B. Zhang, A. Korolj, B.F.L. Lai, M. Radisic, Advances in organ-on-a-chip engineering, Nat. Rev. Mater. 3 (8) (2018) 257–278.
[53] S.N. Bhatia, D.E. Ingber, Microfluidic organs-on-chips, Nat. Biotechnol. 32 (8) (2014) 760–772.
[54] N. Ashammakhi, E. Elkhammas, A. Hasan, Translating advances in organ-on-a-chip technology for supporting organs, J. Biomed. Mater. Res. B Appl. Biomater. 107 (6) (2019) 2006–2018.
[55] S.B. Campbell, Q. Wu, J. Yazbeck, C. Liu, S. Okhovatian, M. Radisic, Beyond Polydimethylsiloxane: Alternative Materials for Fabrication of Organ-On-A-Chip Devices and Microphysiological Systems, ACS Biomaterials Science & Engineering, 2020.
[56] J. Nie, Q. Gao, Y. Wang, J. Zeng, H. Zhao, Y. Sun, J. Shen, H. Ramezani, Z. Fu, Z. Liu, M. Xiang, J. Fu, P. Zhao, W. Chen, Y. He, Vessel-on-a-chip with hydrogel-based microfluidics, Small 14 (45) (2018) 1802368.
[57] D. Chimene, C.W. Peak, J.L. Gentry, J.K. Carrow, L.M. Cross, E. Mondragon, G. B. Cardoso, R. Kaunas, A.K. Gaharwar, Nanoengineered ionic–covalent entanglement (NICE) bioinks for 3D bioprinting, ACS Appl. Mater. Interfaces 10 (12) (2018) 9957–9968.
[58] D.J. Shiwarski, A.R. Hudson, J.W. Tashman, A.W. Feinberg, Emergence of FRESH 3D printing as a platform for advanced tissue biofabrication, APL Bioengineering 5 (1) (2021), 010904.
[59] C.S. O'Bryan, T. Bhattacharjee, S.L. Marshall, W. Gregory Sawyer, T.E. Angelini, Commercially available microgels for 3D bioprinting, Bioprinting 11 (2018), e00037.
[60] K.J. LeBlanc, S.R. Niemi, A.I. Bennett, K.L. Harris, K.D. Schulze, W.G. Sawyer, C. Taylor, T.E. Angelini, Stability of high speed 3D printing in liquid-like solids, ACS Biomater. Sci. Eng. 2 (10) (2016) 1796–1799.
[61] A.K. Grosskopf, R.L. Truby, H. Kim, A. Perazzo, J.A. Lewis, H.A. Stone, Viscoplastic matrix materials for embedded 3D printing, ACS Appl. Mater. Interfaces 10 (27) (2018) 23353–23361.
[62] J.K. Carrow, L.M. Cross, R.W. Reese, M.K. Jaiswal, C.A. Gregory, R. Kaunas, I. Singh, A.K. Gaharwar, Widespread changes in transcriptome profile of human mesenchymal stem cells induced by two-dimensional nanosilicates, Proc. Natl. Acad. Sci. Unit. States Am. 115 (17) (2018) E3905.
[63] J.R. Xavier, T. Thakur, P. Desai, M.K. Jaiswal, N. Sears, E. Cosgriff-Hernandez, R. Kaunas, A.K. Gaharwar, Bioactive nanoengineered hydrogels for bone tissue engineering: a growth-factor-free approach, ACS Nano 9 (3) (2015) 3109–3118.
[64] A. Nojoomi, E. Tamjid, A. Simchi, S. Bonakdar, P. Stroeve, Injectable polyethylene glycol-laponite composite hydrogels as articular cartilage scaffolds with superior mechanical and rheological properties, International Journal of Polymeric Materials and Polymeric Biomaterials 66 (3) (2017) 105–114.
[65] D.W. Howell, C.W. Peak, K.J. Bayless, A.K. Gaharwar, 2D nanosilicates loaded with proangiogenic factors stimulate endothelial sprouting, Advanced Biosystems 2 (7) (2018) 1800092.
[66] C. Sears, E. Mondragon, Z.I. Richards, N. Sears, D. Chimene, E.P. McNeill, C. A. Gregory, A.K. Gaharwar, R. Kaunas, Conditioning of 3D printed nanoengineered ionic–covalent entanglement scaffolds with iP-hMSCs derived matrix, Advanced Healthcare Materials (2020) 1901580, n/a(n/a).
[67] H.P. Lee, G. Lokhande, K.A. Singh, M.K. Jaiswal, S. Rajput, A.K. Gaharwar, Light-triggered in situ gelation of hydrogels using 2D molybdenum disulfide (MoS2) nanoassemblies as crosslink epicenter, Adv. Mater. 33 (23) (2021) 2101238.